Hindawi
Advances in Civil Engineering
Volume 2020, Article ID 8863480, 16 pages
https://doi.org/10.1155/2020/8863480

Research Article

Compression Behavior of CFST Stub Columns with Holes

Yanhua Liu,[1] Qingxin Ren ,[2] and Yuqing Li [1]

[1]*College of Water Conservancy, Shenyang Agricultural University, Shenyang 110866, China*
[2]*School of Civil Engineering, Shenyang Jianzhu University, Shenyang 110168, China*

Correspondence should be addressed to Qingxin Ren; renqingxin@sjzu.edu.cn

Received 10 July 2020; Revised 19 November 2020; Accepted 30 November 2020; Published 12 December 2020

Academic Editor: Andreas Lampropoulos

Holes are always opened in the steel tubes during the inspection and revision of initial concrete imperfections in concrete filled steel tubular (CFST) columns. The structural performance of such composite columns with holes may have obvious differences in comparison with normal CFST members. This paper intends to investigate the influences of sectional type, holes location, holes size, and holes depth on CFST stub columns. The typical failure modes, load-deformation responses, the ultimate strength, and ductility were discussed in detail. A total of twenty-eight specimens, twenty CFST columns with holes, four intact CFST specimens, and four reference hollow steel tubes subjected to axial compressive loading, were tested. The experimental results were compared with predictions of Eurocode 4 and finite element analysis. An empirical equation for predicting the ultimate strength of CFST stub columns with holes was proposed.

1. Introduction

Concrete filled steel tubular (CFST) columns have been widely used in engineering structures, such as high-rise buildings, arch bridges, and high transmission towers. During the constructional process of the huge structures, holes are always opened in the steel tubes to facilitate pouring concrete and improve the efficiency of CFST columns, shown in Figure 1. Although the holes are refilled and mended, the repair process of steel tube will lead to imperfections, which were known as geometrical irregularities. Geometric imperfections refer to deviations from perfect or normal geometry, which may include the size and shape of imperfections resulting from manufacturing, handling, and damage during installation and service, dents, and regular undulation of steel tube.

Since the 1960s, many researches have focused on the prediction for geometric imperfections of metal shells structures. Arbocz and Babcock [1] carried out complete imperfection surveys and traced the growth of the initial imperfections during the loading process and determined the effect of general initial imperfections on the buckling load of cylindrical shells under axial compression. Teng and Rotter [2] addressed the problem of elastic unstiffened thin cylinders with axisymmetric imperfections, which were common in civil engineering structures, and investigated the effects of sinusoidal, local inward and outward imperfections. Tutuncu and Rourke [3, 4] carried out full-scale laboratory tests and performed finite element simulations of cylindrical steel members with both small- and large-scale geometric imperfections. The compression behavior of nonslender cylindrical steel members was quantified and recommendations were made with respect to the imperfection effects on the load capacity. In recent years, the buckling modes and strength of the cylinders with imperfections had been also investigated. Jullien and Limam [5] investigated the effects of the shape, the dimensions, the location, and the number of openings to the buckling of cylindrical shells under axial compression. The experimental and numerical studies indicated that the critical load is sensitive to the opening angle or circumferential size of the hole. Vaziri et al. [6] presented the linear eigenvalue buckling analysis model of singly and doubly cracked cylindrical shells combined internal pressure and axial compression to study the effect of crack on the buckling behavior of cylindrical shells. Prabu et al. [7] gave a parametric study on the buckling behavior of dented short carbon steel cylindrical shell subjected to uniform axial compression.

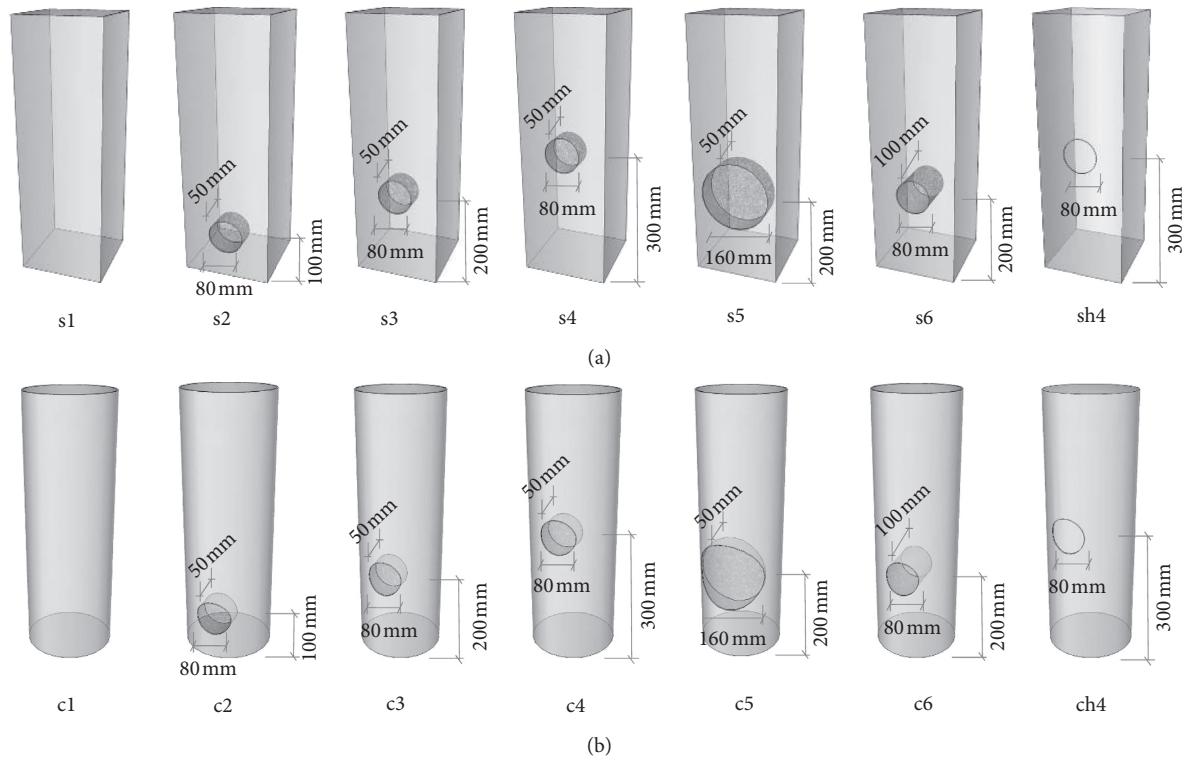

Figure 1: Schematic views of the CFST columns with hole. (a) Square section. (b) Circular section.

Ghanbari Ghazijahani et al. [8] examined the effect of different types of dent imperfections on the plastic buckling capacity and the failure modes of short steel tubes under axial compression.

Compared with the extensive studies carried out on metal shells or hollow tubes with geometric imperfections, very limited research has been conducted on the CFST composite members with notch or dent imperfections in the steel tubes. Tao et al. [9] introduced a function with the shape of initial geometric imperfections for steel plates into numerical model to calculate the ultimate strength of CFST stub columns. Yu et al. [10] investigated the effects of concrete strength, notched holes, or full-perimeter notched slots of the steel tube and different loading conditions on the ultimate capacity and the load-deformation behavior of the concrete filled steel tube (CFST) stub columns. The comparisons were made between the experimental results of the unnotched specimens with the predicted ultimate capacities using Eurocode 4. Chang et al. [11] conducted a parametric study including the notch length, notch orientation, concrete strength, and steel ratio on CFST stub columns. Based on the experimental results, they discussed the load-displacement responses, column strength, and confining effects of the CFST stub columns with artificial notches in the steel tubes and also proposed an empirical equation for predicting the column strength. Tao et al. [12] presented a photogrammetric method to capture the initial imperfections of concrete filled stainless-steel tubular (CFSST) columns in fire and after fire exposure. They developed a three-dimensional finite element (FE) model of CFSST columns and introduced an amplification factor to consider the initial geometric imperfection as the first buckling mode shape of the column.

2. Experimental Investigation

2.1. Specimens Preparation. A total of twenty-eight specimens were tested in the program, twenty CFST columns with holes, four reference intact CFST, and four hollow steel tubes, for comparison purpose. Figures 1(a) and 1(b) give the schematic views of holes location, holes size, and holes depth for CFST columns with square and circular cross section, respectively. These holes were artificially made in the process of preparing the specimen. A summary of the specimens is listed in Table 1, where the specimens naming rules are characterized as follows: The initial character "s" or "c" stands for the square or circular section, respectively. The following character "s" or "h" (if any) stands for the holes only in the steel tube or the hollow section without concrete infill, respectively. The first number stands for the different group with the same column specimen type, and the second number stands for the order of specimens in the same group. All specimens had a same length (L) of 600 mm. The average width (B) of the square cross section and the overall diameter (D) of the circular section both were 200 mm. The average tube thickness (t) is 2.92 mm. The characters h, d, and l are the testing parameters, where h is designated as the holes height, d represents the holes size, and l is holes depth. At present, there is no specific requirement for the opening size of CFST in China. Only the section loss rate of the opening in the steel tube wall should not be more than 50%. It is only required that cross section loss rate should not be greater

Table 1: Parameters of the tested CFST column.

Sectional type	No.	Specimen label	B (D) × t (mm)	L (mm)	h (mm)	d (mm)	l (mm)	N_{ue} (kN) Measured	N_{ue} (kN) Average	SI Measured	SI Average	DI Measured	DI Average	Eurocode 4 (2004) N_{EC4}/kN	Eurocode 4 (2004) N_{EC4}/N_{ue}
Square	1	s1-1	□-200 × 2.92	600				3074	3100	0.992	1.000	1.224	1.217	2914	0.948
	2	s1-2	□-200 × 2.92	600				3125		1.008		1.209		2914	0.932
	3	s2-1	□-200 × 2.92	600	100	80	50	2894	2898	0.934	0.935	1.155	1.154	2621	0.906
	4	s2-2	□-200 × 2.92	600	100	80	50	2901		0.936		1.152		2621	0.903
	5	s3-1	□-200 × 2.92	600	200	80	50	2805	2852	0.905	0.920	1.133	1.136	2621	0.934
	6	s3-2	□-200 × 2.92	600	200	80	50	2899		0.935		1.138		2621	0.904
	7	s4-1	□-200 × 2.92	600	300	80	50	2736	2782	0.883	0.897	1.113	1.119	2621	0.958
	8	s4-2	□-200 × 2.92	600	300	80	50	2827		0.912		1.124		2621	0.927
	9	s5-1	□-200 × 2.92	600	200	160	50	2300	2291	0.742	0.739	1.118	1.105	2329	1.013
	10	s5-2	□-200 × 2.92	600	200	160	50	2282		0.736		1.092		2329	1.021
	11	s6-1	□-200 × 2.92	600	200	80	100	2749	2682	0.887	0.865	1.113	1.099	2407	0.876
	12	s6-2	□-200 × 2.92	600	200	80	100	2615		0.844		1.086		2407	0.920
	13	sh4-1	□-200 × 2.92	600	300	80		786	773	0.254	0.249	1.094	1.083	—	
	14	sh4-2	□-200 × 2.92	600	300	80		759		0.245		1.071			
								Mean							0.941
								Standard deviation							0.089
Circular	15	c1-1	○-200 × 2.92	600				2721	2713	1.003	1.000	2.413	2.632	2573	0.946
	16	c1-2	○-200 × 2.92	600				2705		0.997		2.851		2573	0.951
	17	c2-1	○-200 × 2.92	600	100	80	50	2452	2433	0.904	0.897	2.046	2.028	2201	0.898
	18	c2-2	○-200 × 2.92	600	100	80	50	2413		0.889		2.011		2201	0.912
	19	c3-1	○-200 × 2.92	600	200	80	50	2354	2332	0.868	0.860	1.984	1.910	2201	0.935
	20	c3-2	○-200 × 2.92	600	200	80	50	2310		0.851		1.836		2201	0.953
	21	c4-1	○-200 × 2.92	600	300	80	50	2230	2255	0.822	0.831	1.726	1.773	2201	0.987
	22	c4-2	○-200 × 2.92	600	300	80	50	2280		0.840		1.819		2201	0.965
	23	c5-1	○-200 × 2.92	600	200	160	50	1849	1843	0.682	0.679	1.593	1.660	1749	0.946
	24	c5-2	○-200 × 2.92	600	200	160	50	1836		0.677		1.727		1749	0.953
	25	c6-1	○-200 × 2.92	600	200	80	100	2043	2105	0.753	0.776	1.634	1.597	1941	0.950
	26	c6-2	○-200 × 2.92	600	200	80	100	2166		0.798		1.560		1941	0.896
	27	ch4-1	○-200 × 2.92	600	300	80		826	837	0.304	0.308	1.666	1.689		
	28	ch4-2	○-200 × 2.92	600	300	80		847		0.312		1.711			
								Mean							0.937
								Standard deviation							0.143

than 50% in accordance with the China Standards CECS188: 2019 [13]. Relevant research results [14] showed that the position of the opening hole is more suitable at the bottom of the column. Therefore, the holes height ($h = 100$ mm, 200 mm, and 300 mm), the holes size ($d = 80$ mm and 160 mm), and the holes depth ($l = 50$ mm and 100 mm) were selected as shown in Figure 1. N_{ue} is the measured ultimate load, and SI and DI are a strength index and a ductility index, which are defined in the following sections of this article.

In fabricating the tubes, steel sheets were cut according to their required dimensions and cold-formed U-shaped steel channels, and then two such U-shaped steel tubes were welded together to form a square tube. One precut steel plate was wrapped first and welded to form a circular tube. Prior to the welding, a hole of 80 mm or 160 mm was marked and drilled on a target location in the surface of each steel tube. An optimized drilling process was chosen to minimize the potential drilling imperfections. After the drilling, no obvious induced deformation was found in the tubes. Two end plates with a thickness of 20 mm were welded to the top and bottom ends of each steel tube. Self-consolidating concrete (SCC) was filled into steel tube without any vibration. Before casting, predrilled holes of the steel tube were inserted by wooden cylinders with 80 mm or 160 mm diameter and 50 mm or 100 mm length. These wooden cylinders were used for each specimen to form the target hole of inner concrete and prevent the concrete overflowing.

2.2. Material Properties. Three tensile coupons for each type of steel tubes were conducted to determine the material properties. The specimens for square steel tubes were extracted from their flat surfaces, whereas the specimens for circular steel tubes were taken from the original steel tubes in longitudinal direction. Due to the fact that the difference of yield and ultimate strengths between the two types of steel tubes was less than 1%, in convenience, the average steel material properties values were adopted in the paper. The measured yield strength (f_y), ultimate strength (f_u), modulus of elasticity (E_s), and Poisson's ratio (μ_s) of the steel tube were 389.3 MPa, 532.1 MPa, 206,000 N/mm^2, and 0.294, respectively.

Self-consolidating concrete (SCC) was cast in the laboratory. The mix proportions by mass were as follows: cement (380 kg/m^3), fly ash (170 kg/m^3), water (176 kg/m^3), sand (850 kg/m^3), coarse aggregate (850 kg/m^3), and additional high-range water reducer (13.6 kg/m^3). The measured modulus of elasticity (E_c) of the concrete was 35,000 MPa. Concrete cubes were cast and tested to determine the compressive strength (f_{cu}) of the concrete. The average compressive strengths at 28 days and at the time of the tests were 61.4 MPa and 62.8 MPa, respectively.

2.3. Test Setup and Instrumentation. The test apparatus for the present experimental program was a 5000 kN loading capacity universal testing machine. Figure 2(a) gives a schematic view of the test setup, while Figures 2(b) and 2(b) show the photos of columns during testing. The column specimens were placed into the testing machine and the loads were applied on the specimens directly, as shown in Figure 3. A total of fourteen strain gauges were attached to four sides of each CFST specimen with holes, as shown in Figure 2, in which eight strain gauges were attached symmetrically at the four sides of a hole, while the other six strain gauges were located at the other three steel tube surfaces on the same height of the hole to record the strain values of the test samples. Two displacement transducers were symmetrically fixed on the bottom plate to measure the axial deformations.

The load was applied in small increment of approximately one-tenth of the estimated ultimate strength and maintained for two minutes at each load increment. After the column started to buckle, the load increment was reduced to about one-twentieth of the estimated ultimate strength. At each increment stage of loading, the strain and deformation measurements were recorded. Generally, the loading was terminated when one of the circumstances was reached: (1) axial load fell to below 65% of the peak load; (2) weld failure occurred; or (3) average strain of the specimen ($=\Delta/H$, Δ is the axial deformation) reached 20,000 $\mu\varepsilon$.

3. Experimental Results and Discussion

3.1. Failure Modes. The typical failure appearances of CFST columns with holes are shown in Figure 3, which indicate that CFST columns with holes demonstrated a different failure mode compared to the intact column. As expected, the intact specimen showed outward local buckling in the tubes near the mid-height of the specimens. For specimens with holes, deformations were initiated from the area around holes, and then the cracking of steel tube could be observed and developed accompanied with outward buckling near hole. The effect of holes size on buckling and failure mode was not considerable for the specimens with holes. However, the failure modes of CFST columns with holes were quite different with the reference hollow steel tubular columns with holes. When reaching the ultimate strength, inward local buckling occurred near the hole for hollow steel tubular members. Meanwhile, for CFST specimens with holes, inward tube buckling was prevented due to the existence of the concrete core; thus only outward buckling was observed, as shown in Figure 3. Like the intact columns, outward local buckling of the steel tube in square specimens was more obvious than that in circular specimens of CFST columns with holes.

In order to investigate the failure pattern of the concrete core in CFST columns with holes, the steel tubes were removed after the tests. Exposed views of the concrete core were illustrated in Figure 4. For the intact specimens, concrete crushing always existed near the middle of the concrete core. However, for CFST columns with holes, the concrete crushing only occurred near the hole and no obvious concrete damage could be observed at the middle of the concrete core. This may be due to the fact that the lower confining effect could be provided by the opening steel tube to the concrete core near the hole.

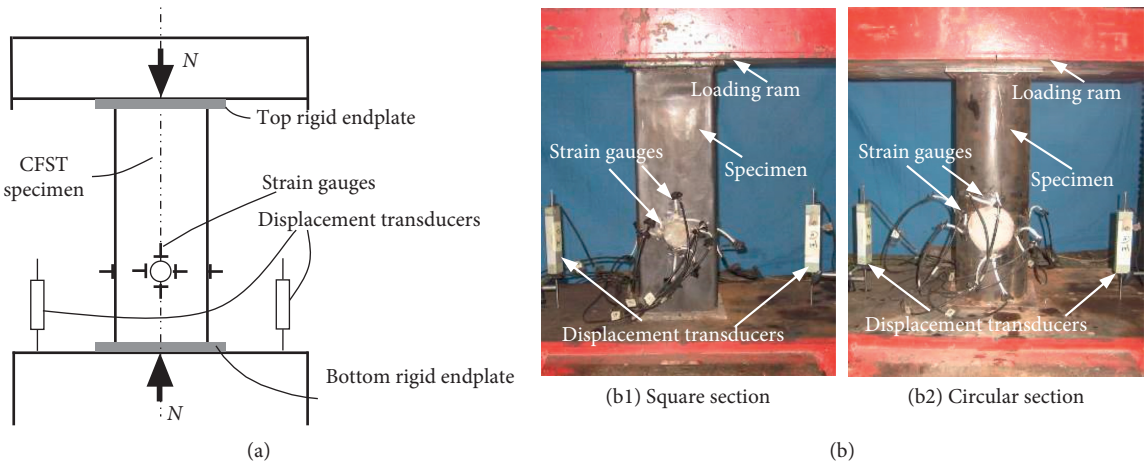

Figure 2: Test setup for opening CFST columns. (a) Schematic view. (b) Photo during test.

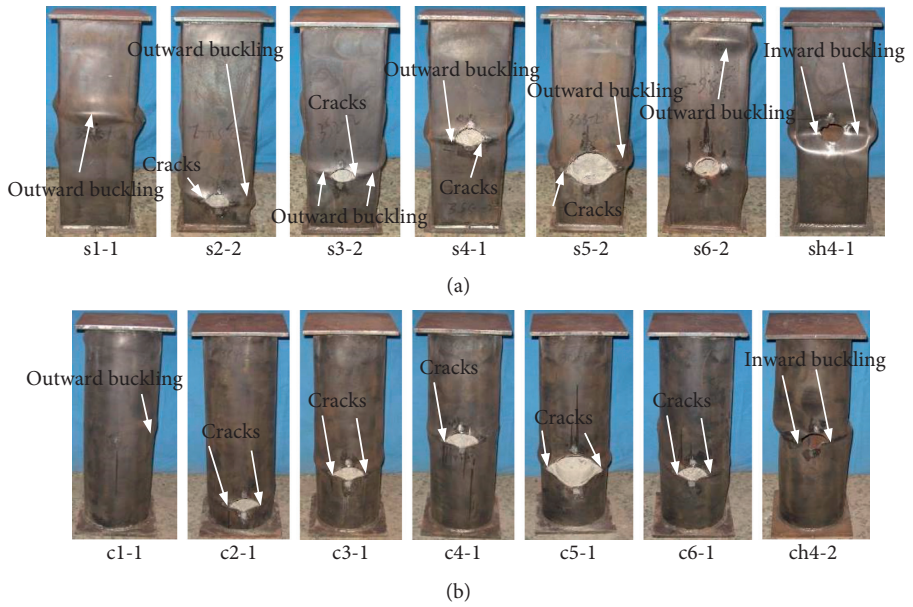

Figure 3: Typical failure modes of opening CFST columns. (a) Square section. (b) Circular section.

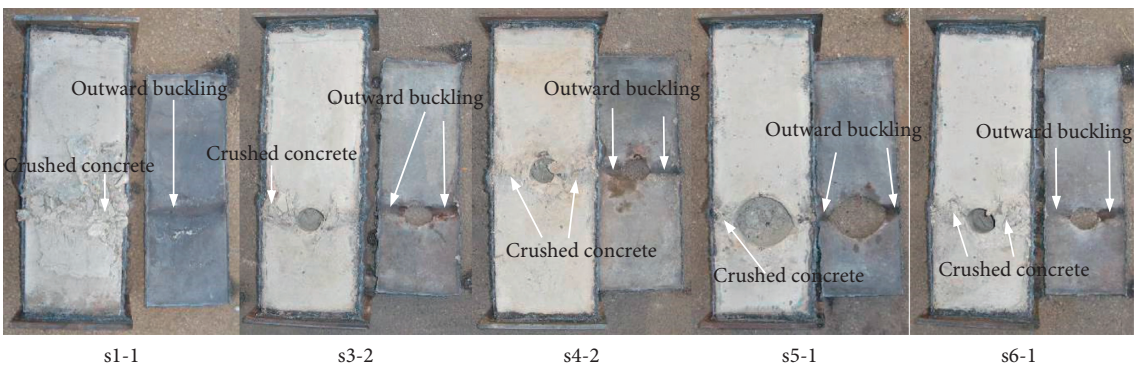

Figure 4: Continued.

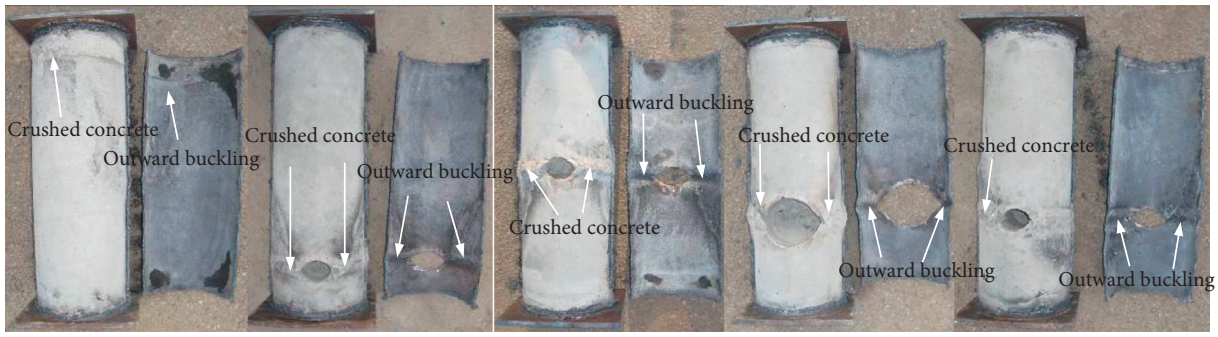

(b)

Figure 4: Typical failure modes of the concrete core. (a) Square section. (b) Circular section.

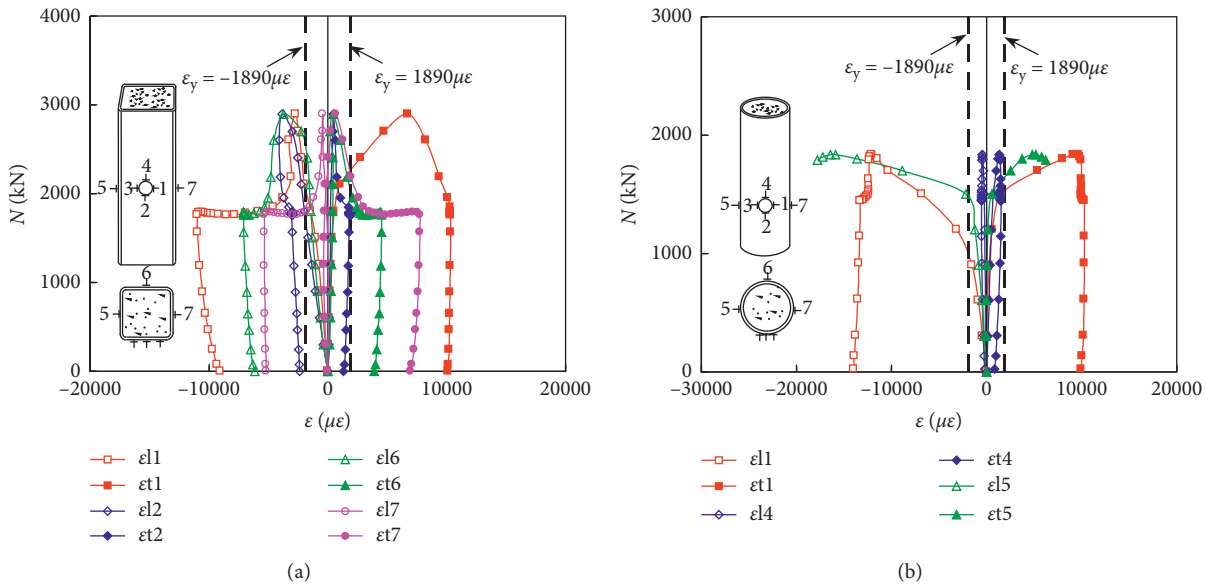

Figure 5: Typical load (N) versus strain ($e\varepsilon$) relations of the tested columns. (a) Square section (s4-1). (b) Circular section (c3-1).

3.2. Axial Load versus Axial Strain Curves. The typical measured loads (N) versus strain (ε) relations of an opening square section column specimen (s4-1, in which the holes height $h = 300$ mm, the holes size $d = 80$ mm, and the holes depth $l = 50$ mm) and the circular one (c3-2, in which the holes height $h = 200$ mm, the holes size $d = 80$ mm, and the holes depth $l = 50$ mm) are shown in Figures 5(a) and 5(b), where ε_l and ε_t stand for longitudinal and transverse strain, respectively; ε_y stands for the steel yield strain. In these figures, the compressive strains are denoted as positive and the tensile ones as negative. For each member, the N-ε relation curves at multiple locations are displayed, including two sides of an opening, where the positions are denoted as number 1 and number 2 (ε_{l1}, ε_{l2}, ε_{t1}, and ε_{t2}), and the other two surfaces on the same height, named as number 5 and number 6 (ε_{l5}, ε_{l6}, ε_{t5}, and ε_{t6}).

For the square specimen s4-1, it could be obtained from Figure 5(a) that the longitudinal strain ε_{l1} and transverse strain ε_{t1} were significantly larger than the other longitudinal and transverse strains. The reason was that the position was located at Sections 1–3, where was the most dangerous location for columns under the axial compressive loading due to the cutouts of the steel tube. A significant crack and outward buckling were observed at this position, which was shown in Figure 5. When N_{ue} was reached, the longitudinal strains ε_{l2}, ε_{l6}, and ε_{l7} were 453 $\mu\varepsilon$, 465 $\mu\varepsilon$, and 667 $\mu\varepsilon$, respectively. The transverse strains ε_{t2}, ε_{t6}, and ε_{t7} were −3843 $\mu\varepsilon$, −3713 $\mu\varepsilon$, and −425 $\mu\varepsilon$, respectively. It is indicated that there were a little smaller longitudinal strain and a larger transverse strain in position 2, which were the axial direction side of the hole. This may be due to the fact that when the outward buckling occurred in Sections 1–3, the axial direction would be squeezed, and the longitudinal strain decreased and the transverse strain increased.

For the circular specimen c3-1, comparisons of the strain values at different locations could be obtained from Figure 5(b). When the ultimate strength N_{ue} was attained, the longitudinal strains ε_{l1}, ε_{l4}, and ε_{l5} were 9098 $\mu\varepsilon$, 1315 $\mu\varepsilon$, and 4827 $\mu\varepsilon$, while the corresponding transverse strains at each section (ε_{t1}, ε_{t4}, and

ε_{t5}) were −12503 $\mu\varepsilon$, −438 $\mu\varepsilon$, and −15883 $\mu\varepsilon$, respectively. It could be seen that the longitudinal strain value on position 1 and the transverse strain of position 5 were higher than those on position 4, which indicated that the buckling deformation was noticeably larger at the mentioned positions than at position 4 under the same load level during the testing. This was consistent with the observed failure mode for CFST specimen c3-1, where the outward buckling and crack were generally located at this position.

3.3. Axial Load versus Axial Deformation Relations. The effect of different holes height on the measured load (N) versus deformation (Δ) curves for the specimens was shown in Figures 6(a) and 6(b) for square and circular specimens, respectively. In the figures, the deformations (Δ) were recorded by two displacement transducers and the average value of two readings was used to represent Δ. From Figure 6, the influence of holes height on the initial slope of N-Δ curves and the load-carrying capacities were minor. The ultimate load N_{ue} of specimens had a little decrease with the increase of the holes height from 100 mm to 300 mm. This may be due to the fact that the failure position was always near the mid-height of CFST columns, which could weaken the confining effect of the steel tube with the holes height increasing (the height of the columns was 600 mm, so it was nearer to the mid-height when the holes height increased).

However, significant influence of holes size (d) on both load-carrying capacities and ductility could be found in CFST columns with holes, as can be seen in Figure 7. For square specimens, the average ultimate loads N_{ue} with holes size (d) of 80 mm and 160 mm were 2852 kN and 2291 kN, respectively, while the average ultimate load N_{ue} for normal CFST columns was 3100 kN. The strength of CFST columns with the holes size (d) of 80 mm and 160 mm reduced by 8.0% and 26.1% compared with normal CFST columns due to the weaker confining effect of the steel tube. For circular specimens, the average ultimate load N_{ue} decreased from 2332 kN to 1843 kN by increasing the holes size (d) from 80 mm to 160 mm. The strength decreased by 14.0% and 32.1% compared with normal CFST columns. This indicated that the mechanical behavior would be weakened with increasing the holes size, regardless of the sectional type.

The influence of holes depth (l) on the load-carrying capacities of CFST columns with holes was not as obvious as that of holes size (d) as can be seen from Figure 8. For square specimens, drilling holes on the inner concrete would lead to a strength reduction of 8.0% and 13.5% compared with normal CFST columns. For circular specimens, the average ultimate load N_{ue} decreased from 2332 kN to 2105 kN by increasing the holes depth (l) from 50 mm to 100 mm, which decreased the strength by 14.0% and 22.4% compared with normal CFST columns.

Figures 9(a) and 9(b) compared the axial load (N) and axial deformation (Δ) curves of the opening CFST columns with concrete or without concrete infill (hollow section members). From Figure 9, the initial slope of N-Δ curves and the ultimate load N_{ue} of the CFST columns with hole were dramatically higher than those of unfilled columns. The reason was that the inward local buckling of steel tube could be prevented by the infilled concrete, which was similar to the results of normal CFST columns without holes.

3.4. Ultimate Strength. The measured ultimate strength N_{ue} for each CFST specimen is listed in Table 1, where N_{ue} is defined as the peak load. It could be seen from Table 1 that all CFST stub columns with holes had lower values of ultimate strength N_{ue} compared with normal CFST columns. In order to gain a better insight into the influence of the testing parameters on the ultimate strength of the CFST columns with holes, a strength index (SI) defined by Han [15] as shown in equation (1) is used:

$$\mathrm{SI} = \frac{N_{ue}}{N_{ur}}, \tag{1}$$

where N_{ue} is the measured ultimate load (i.e., the peak load) of the column specimens; N_{ur} is the average ultimate load of the benchmarking CFST columns, that is, s1-1 and s1-2 for square section and c1-1 and c1-2 for circular section. The strength indexes (SI) are listed in Table 1 and are plotted in Figure 10 against the holes height (h), holes size (d), and holes depth (l) and for both cases with and without concrete infilled specimens.

From Figure 10(a), it could be found that, for the square columns with the holes height (h) of 100 mm, 200 mm, and 300 mm, the SIs were 0.935, 0.920, and 0.897. The higher of the hole tended to cause a slight lower of SIs. When the holes size (d) of 80 mm and 160 mm, the SIs were 0.920 and 0.739, respectively. The SIs tended to decrease with the increase of the holes size due to the reduced confining effect of steel tube. The SIs were 0.920 and 0.865 with holes depth (l) of 50 mm and 100 mm, which were reduced by the enlargement of the holes depth (l). The SIs of CFST columns with holes (holes height $h = 300$ mm, holes size $d = 80$ mm, and holes depth $l = 50$ mm) with and without concrete infill were 0.897 and 0.249. SI of the CFST columns with hole was 3.6 times that of the hollow steel tubular columns.

For the circular columns as shown in Figure 10(b), the SIs were 0.897, 0.860, and 0.831 with the holes height (h) of 100 mm, 200 mm, and 300 mm, respectively. The holes height had a slight effect on the strength indexes. SI decreased from 0.860 to 0.679 as the holes size (d) increased from 80 mm to 160 mm. The influence of the holes size on the strength index (SI) was significant, and the decrease was more than 21%. When the holes depth (l) was 50 mm and 100 mm, the SIs were 0.860 and 0.776, respectively. The decrease of the holes depth on the strength index (SI) from 50 mm to 100 mm was almost 10%. Meanwhile, SI of the circular CFST columns with hole was 2.70 times that of the hollow steel tubular columns. The influence of the concrete infill on the strength index was quite considerable, which was consistent with that of CFST columns [16].

In order to quantitatively evaluate the effects of h, d, and l on the ultimate strength of CFST stub column with hole, the strength indexes (SIs) versus h, d, and l relations of the tested square and circular columns are shown in Figures 11(a) and 11(b). According to the measured data, empirical formulae of SI with respect to holes height (h), holes size (d), and holes

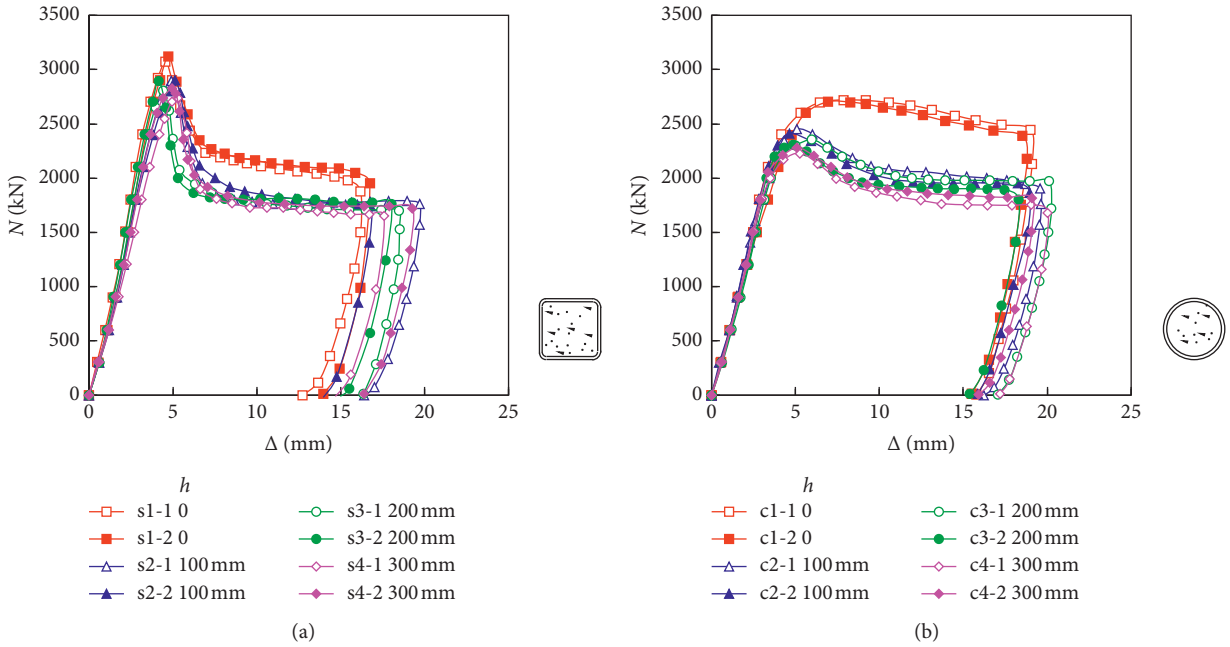

Figure 6: Effects of holes height on load (N) versus deformation (Δ) diagrams. (a) Square section. (b) Circular section.

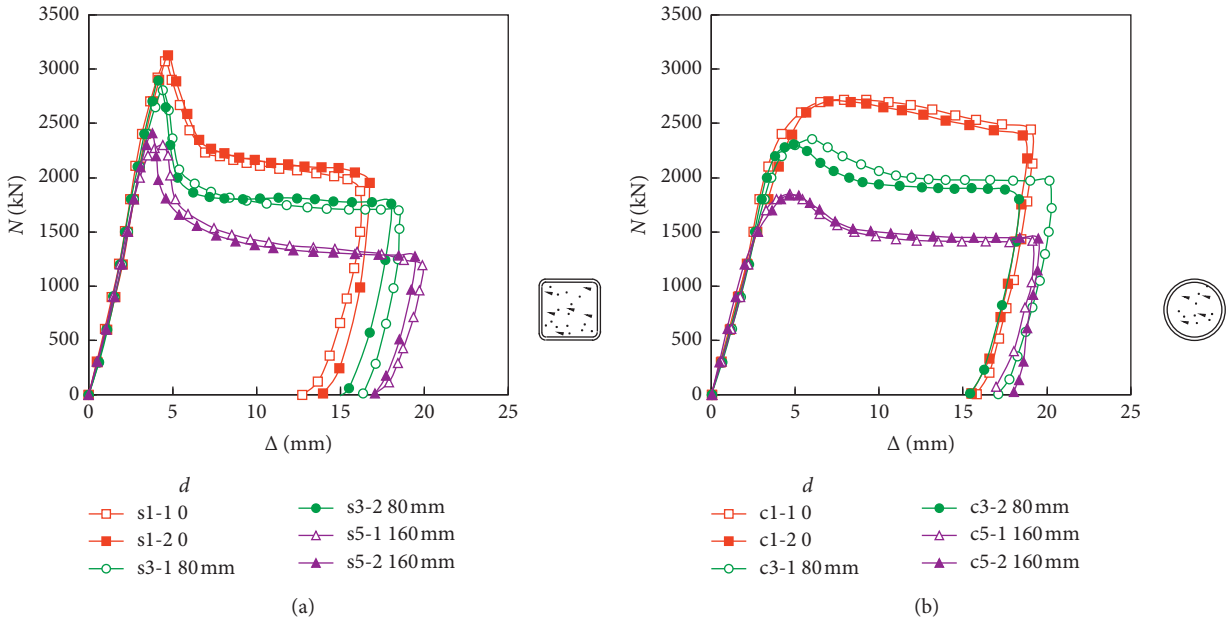

Figure 7: Effects of holes size on load (N) versus deformation (Δ) diagrams. (a) Square section. (b) Circular section.

depth (l) were given and shown in Figure 11. The increase in holes depth and holes size of the steel tube led to the decreasing of the strength of the opening CFST columns. This can be explained by two facts. Firstly, due to the presence of the hole in the CFST columns, the specimen becomes an eccentric-loaded member, and thus its bearing capacity decreases. Secondly, with an increase of the holes depth and holes size, the effective section area decreases, thereby reducing the confining effect and ultimate load.

3.5. Ductility. In order to quantify the effect of different parameters on section ductility of CFST stub columns with holes, a ductility index (DI), which had been used in Han et al. [15], was adopted in this paper. It was defined as

$$\mathrm{DI} = \frac{\Delta_{85\%}}{\Delta_{\mathrm{ue}}}, \tag{2}$$

where $\Delta_{85\%}$ is the axial deformation when the axial load falls to 85% of the ultimate strength and Δ_{ue} is the axial

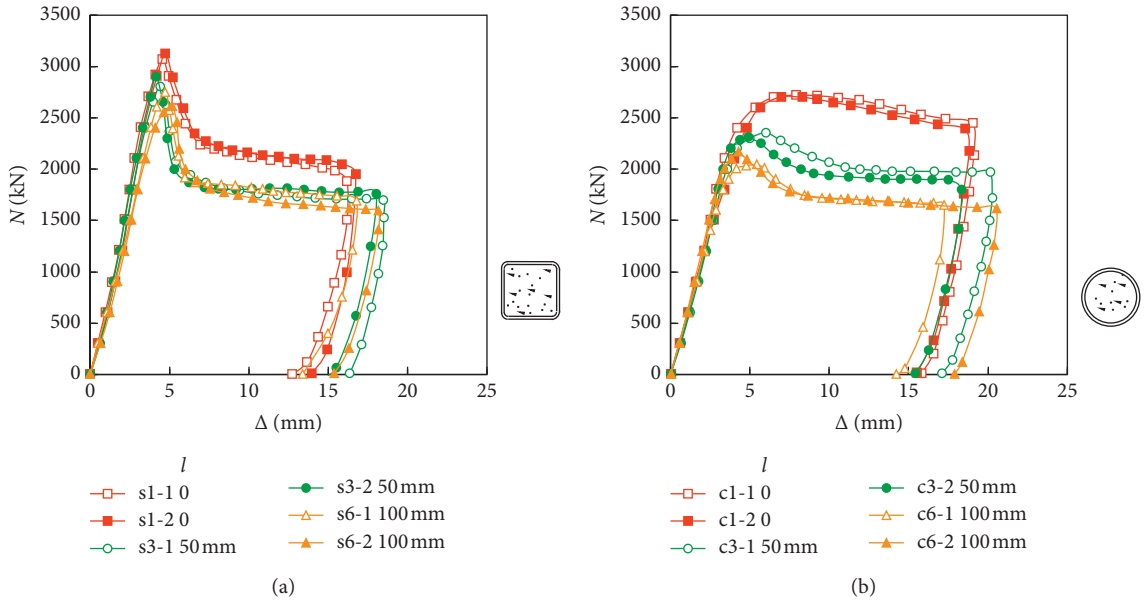

Figure 8: Effects of holes depth on load (N) versus deformation (Δ) diagrams. (a) Square section. (b) Circular section.

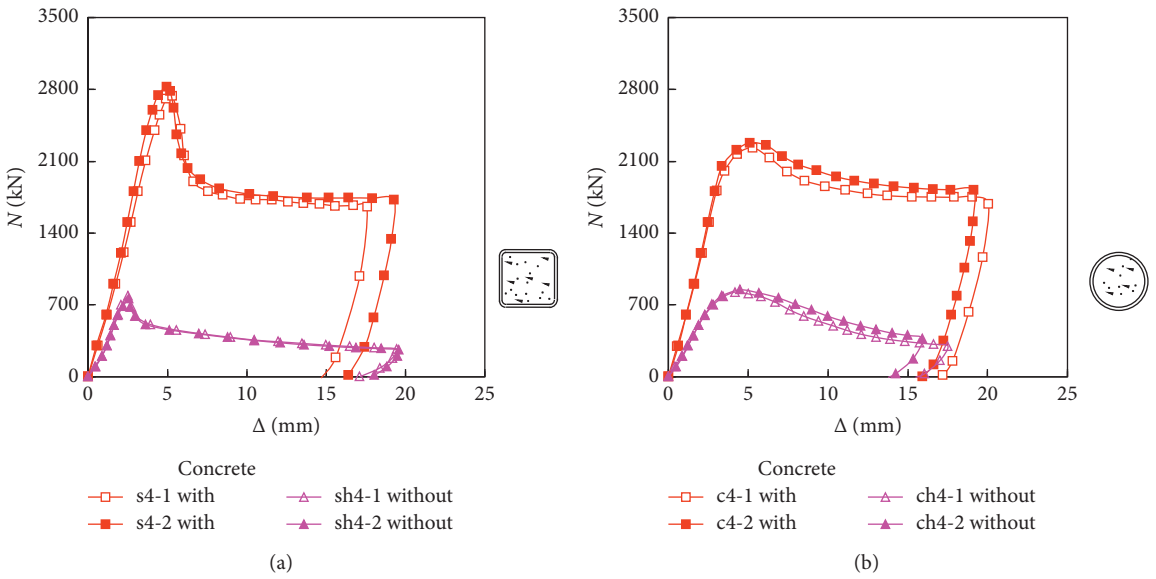

Figure 9: Load (N) versus deformation (Δ) diagrams with or without concrete infill. (a) Square section. (b) Circular section.

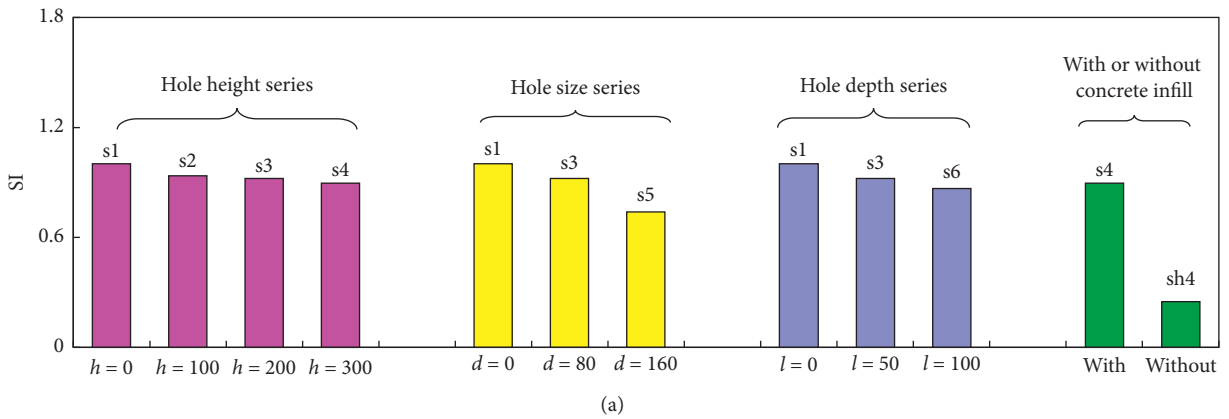

Figure 10: Continued.

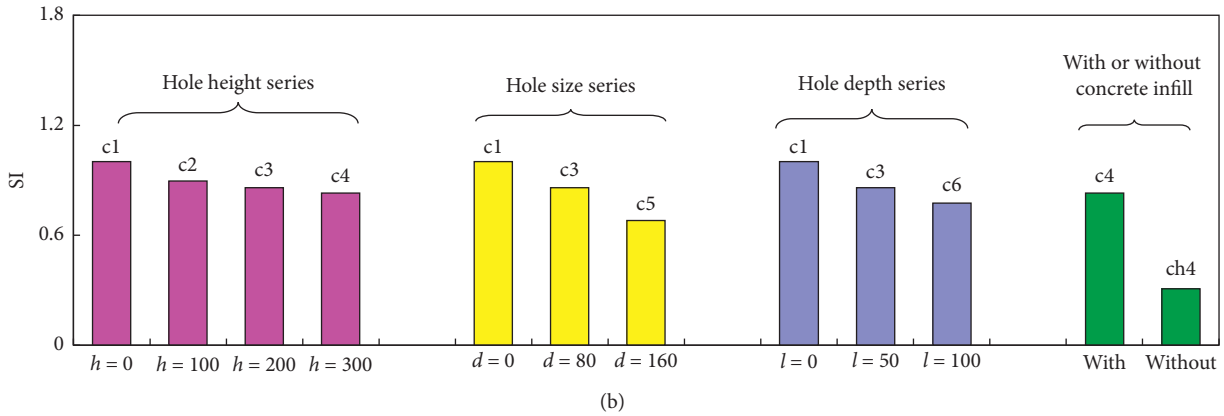

(b)

Figure 10: Strength index (SI) of opening CFST columns. (a) Square section. (b) Circular section.

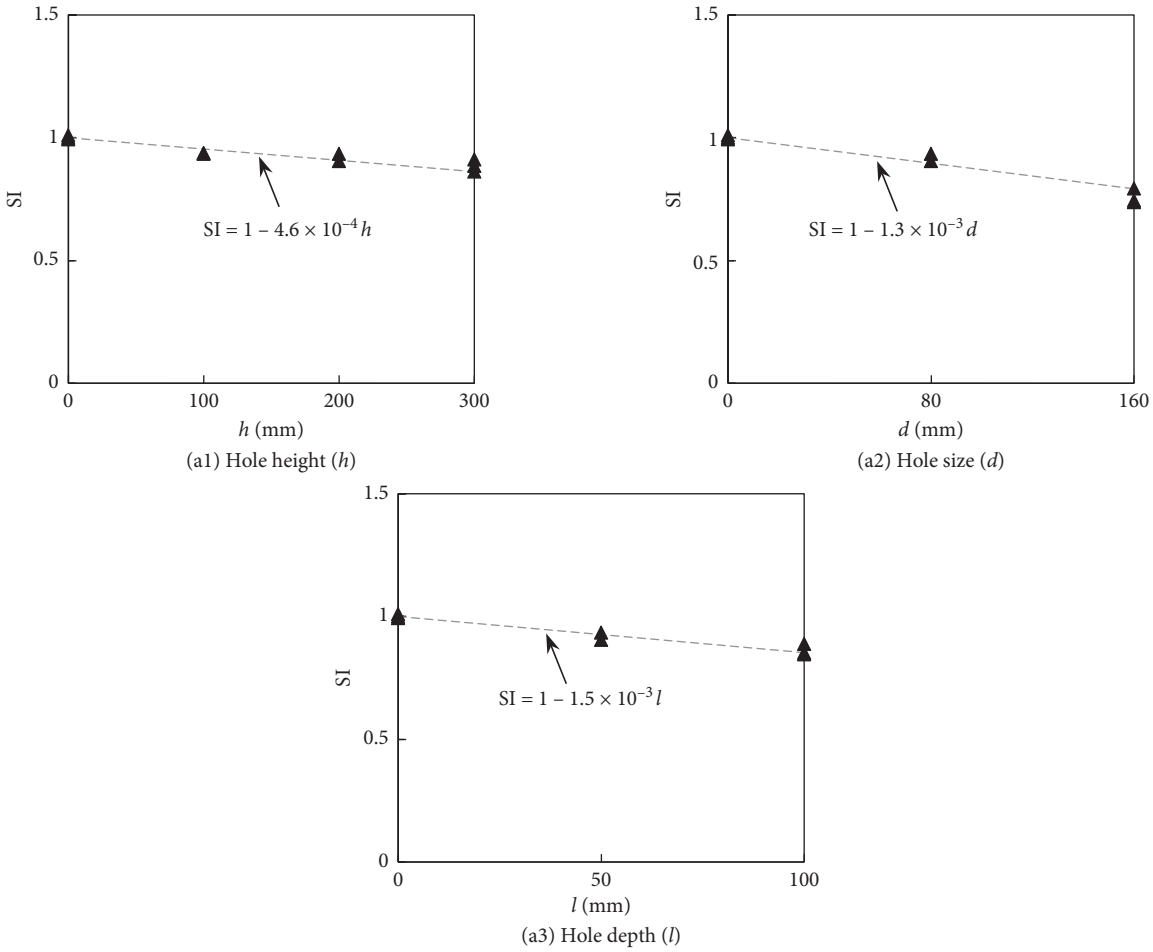

(a1) Hole height (h)

(a2) Hole size (d)

(a3) Hole depth (l)

(a)

Figure 11: Continued.

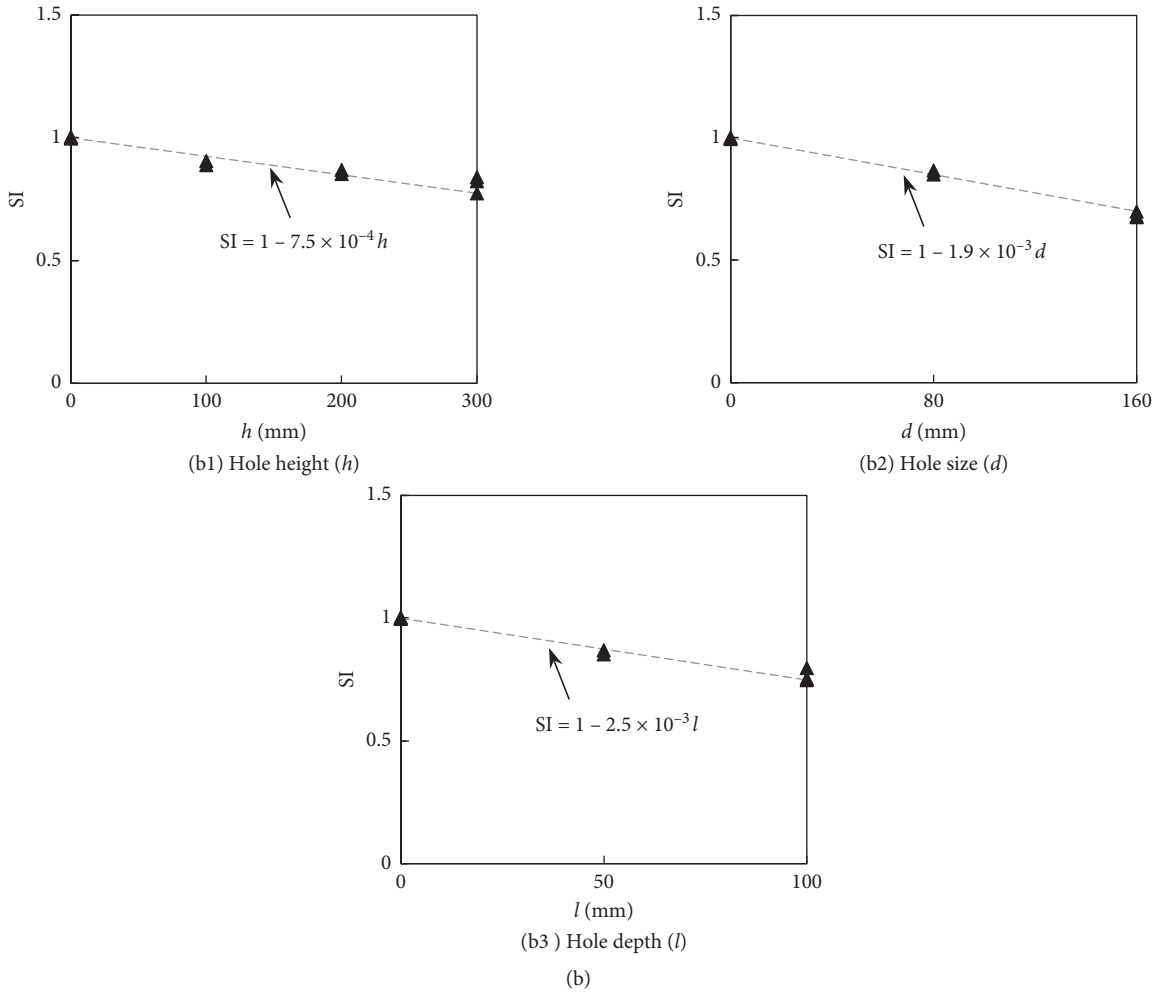

Figure 11: Strength index (SI) versus different parameters relation. (a) Square section. (b) Circular section.

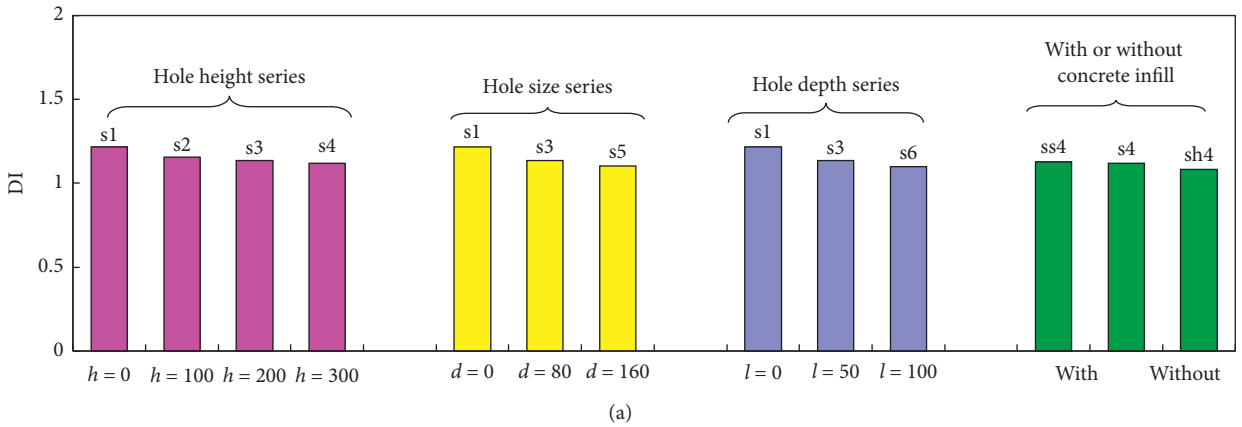

(a)

Figure 12: Continued.

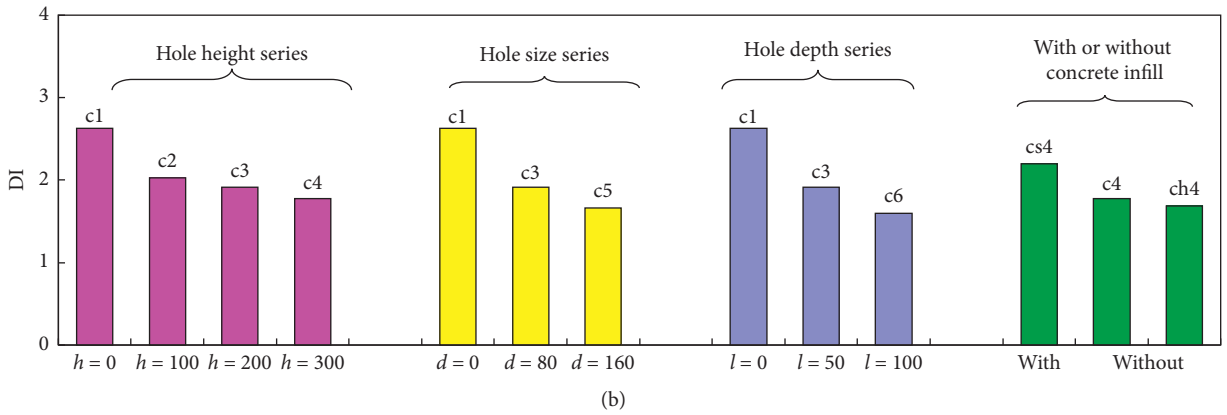

Figure 12: Ductility index (DI) of opening CFST columns. (a) Square section. (b) Circular section.

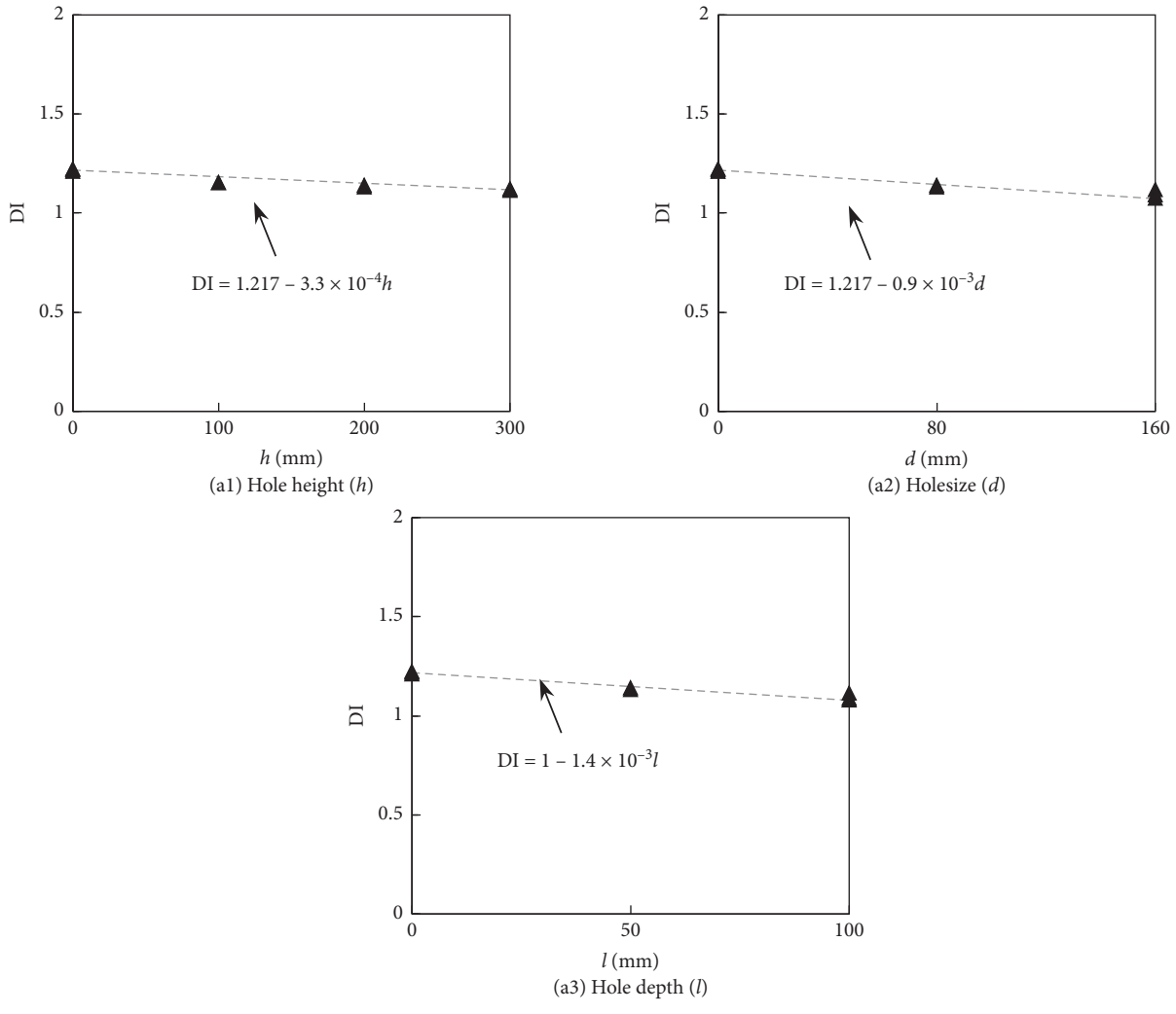

Figure 13: Continued.

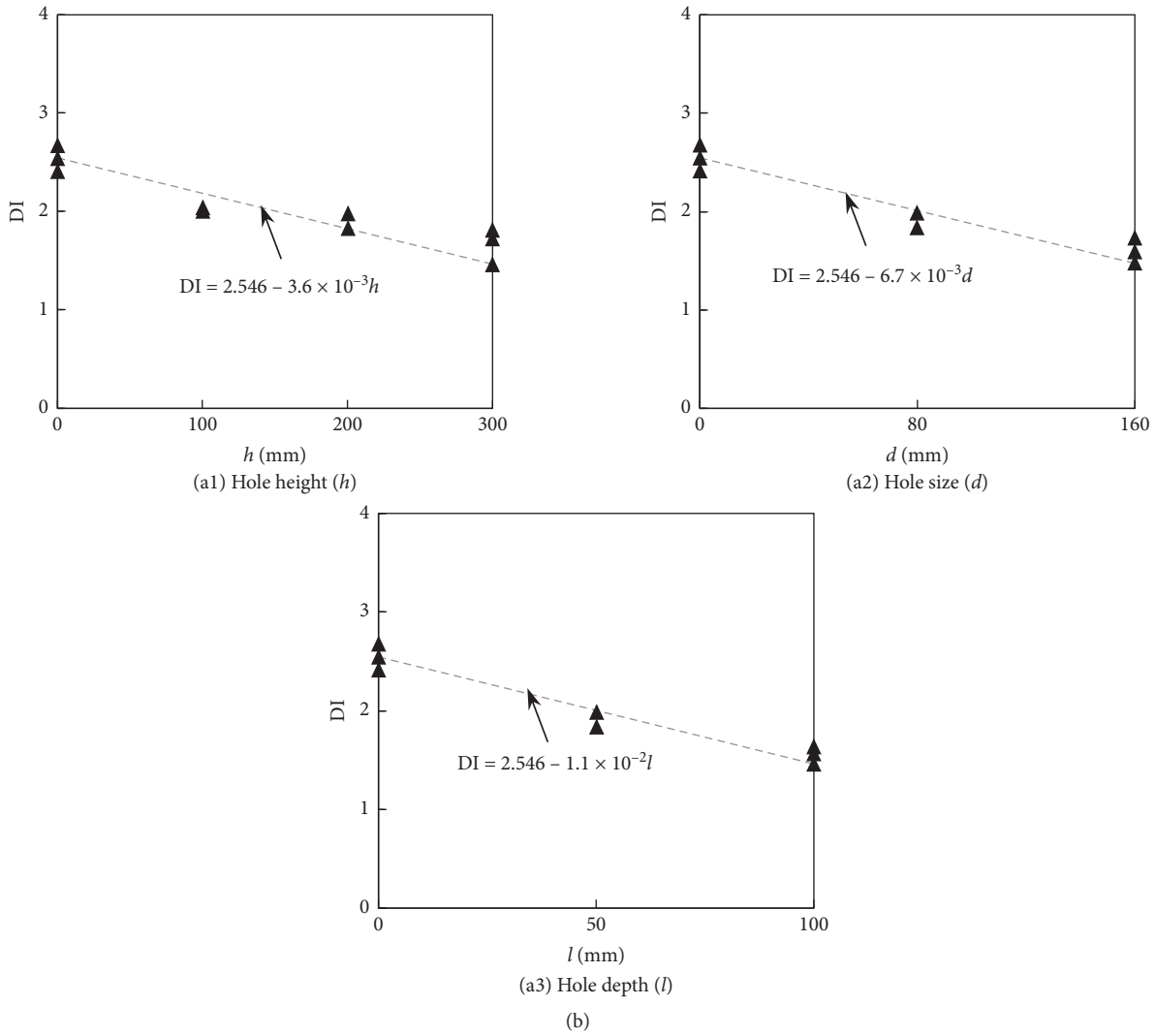

Figure 13: Ductility index (DI) versus different parameters relation. (a) Square section. (b) Circular section.

Table 2: Comparison between predicted capacities and test results for intact CFST column specimens.

Section types	No.	Specimen number	N_{ue} (kN)	AIJ [17]		AISC3610-10 [18]		BS5400 [19]		DBJ13-51-2010 [20]		Eurocode 4 [21]	
				N_{uc} (kN)	N_{uc} (N_{ue})	N_{uc} (kN)	N_{uc} (N_{ue})	N_{uc} (kN)	N_{uc} (N_{ue})	N_{uc} (kN)	N_{uc} (N_{ue})	N_{uc} (kN)	N_{uc} (N_{ue})
Square	1	sc1-1	3074	2572	0.837	2611	0.849	1916	0.623	2835	0.922	2914	0.948
	2	sc1-2	3125	2572	0.823	2611	0.836	1916	0.613	2835	0.907	2914	0.932
Circular	3	cc1-1	2721	2202	0.809	2209	0.812	1966	0.723	2300	0.845	2573	0.946
	4	cc1-2	2705	2202	0.814	2209	0.817	1966	0.727	2300	0.850	2573	0.951

deformation corresponding to the ultimate strength. The evaluated ductility index (DI) so defined is listed in Table 1.

Figure 12 shows the effect of holes height (h), holes size (d), and holes depth (l) on the section ductility of CFST stub columns with holes. For the square columns, the DIs decreased by 1.6% and 1.5% as the holes height increased from 100 mm to 200 mm and to 300 mm. DI decreased by 2.8% as the holes size increased from 80 mm to 160 mm, DI decreased by 3.4% as the holes depth increased from 50 mm to 100 mm, and DI of the CFST columns with holes was 1.03 times that of the hollow steel tube columns with holes. For the circular columns as shown in Figure 12(b), DI decreased by 6.2% and 7.7% as the holes height increased from 100 mm to 200 mm and to 300 mm. DI decreased by 15.1% as the

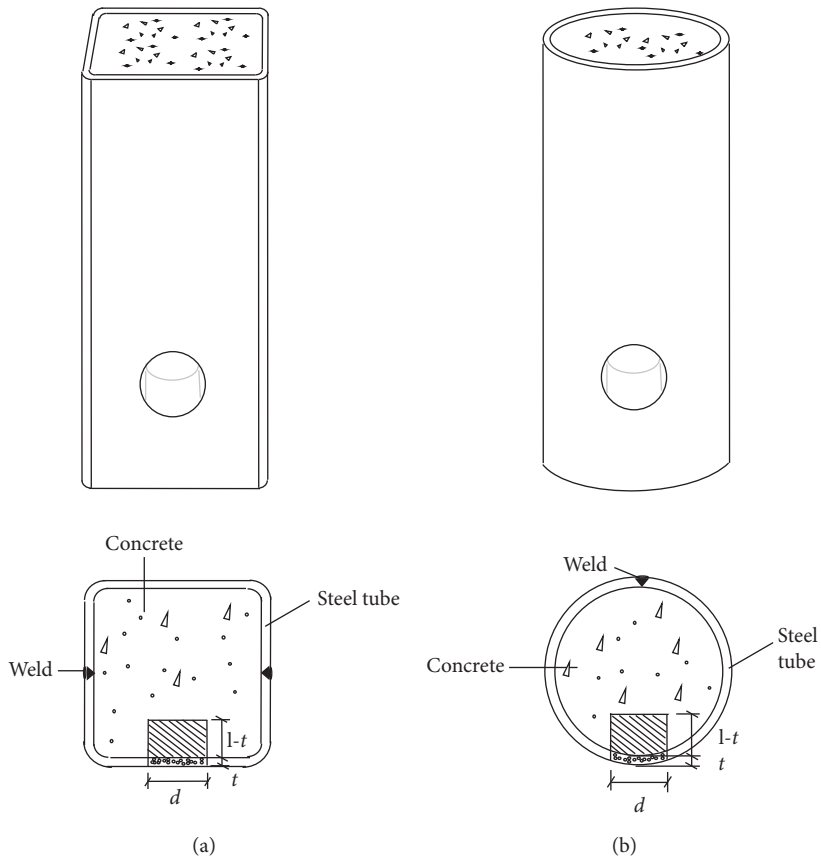

Figure 14: Sketch for the hole in the CFST columns with square section and circular section. (a) Square section. (b) Circular section.

holes size increased from 80 mm to 160 mm. DI decreased by 19.6% as the holes depth increased from 50 mm to 100 mm. DI of the CFST columns with holes was 1.05 times that of the hollow steel tube columns with holes.

By increasing the holes height, holes size, and holes depth, the ductility index (DI) of the specimen was decreased and the initial stiffness was changed compared with the intact one. The holes size and the holes depth have a significant effect on the behavior of the opening CFST columns. This may be due to the fact that the increase of the holes depth and the holes size led to a significant decrease in the effective section area and reduced the confining effect of the steel element, thereby reducing the ductility of the CFST columns. In order to quantitatively evaluate the effects of h, d, and l on the ductility of CFST columns with hole, the ductility indexes (DIs) versus h, d, and l relations of the tested square and circular columns are shown in Figures 13(a) and 13(b), respectively. Empirical formulae of DI with respect to holes height (h), holes size (d), and holes depth (l) are given in Figure 13 based on the measured data.

3.6. Comparison with Code Predictions. A number of design codes, such as AIJ [17], AISC360-10 [18], BS5400-5 [19], DBJ/13-51-2010 [20], and Eurocode 4 [21], can be used to predict the ultimate strength N_{uc} of intact normal CFST columns. The feasibility of these existing codes in the design of CFST columns with holes should be verified.

For CFST stub columns, previous research and the comparison between the tested and predicted intact normal CFST columns with the above design codes have indicated (listed in Table 2) that the ultimate strengths N_{uc} predicted by Eurocode 4 [21] were much closer to the tested ultimate strengths N_{ue} than those by the other design codes. Therefore, only Eurocode 4 [21] is used to predict the ultimate strength of CFST columns with hole in this paper.

For square and circular CFST stub columns, equations (3) and (4) are proposed in Eurocode 4 [21] to predict the ultimate strength:

$$N_{uc} = f_y A_s' + f_c' A_c, \tag{3}$$

$$N_{uc} = \eta_s f_y A_s' + \left(1 + \frac{\eta_c . t}{D} . \frac{f_y}{f_c'}\right) . f_c' A_c, \tag{4}$$

where A_s' is cross-sectional area of steel tube; A_c is cross-sectional area of concrete core; f_c' is the cylinder strength of concrete; η_s and η_c are factors to consider the effect of concrete supposed by Tao [22].

Due to the obvious effects of the size of hole and the depth of the hole on the tested ultimate strength of CFST columns with hole, the parameters of hole size and hole depth were introduced in equations (3) and (4), which can be expressed as equations (5) and (6), respectively:

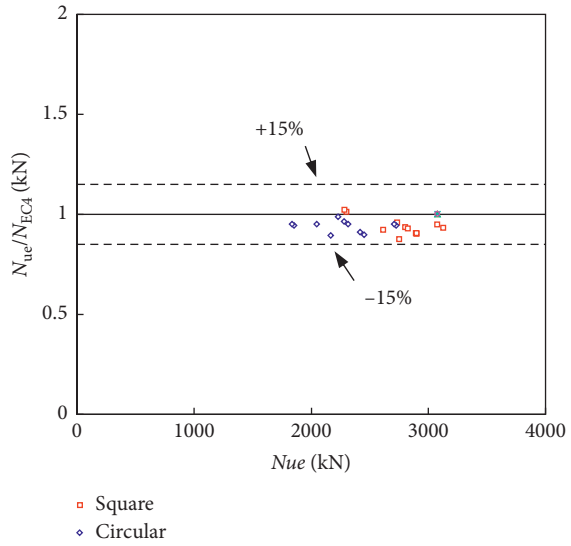

Figure 15: Comparison between test results and EC4 predictions.

$$N_{uc} = f_y\left(A_s - A_{s,cut}\right) + f_c'\left(A_c - A_{c,cut}\right), \tag{5}$$

$$N_{uc} = \eta_s f_y\left(A_s - A_{s,cut}\right) + \left(1 + \frac{\eta_c . t}{D} . \frac{f_y}{f_c'}\right) . f_c'\left(A_c - A_{c,cut}\right), \tag{6}$$

where $A_{c,cut}$ is the largest cross-sectional area of steel tube at the opening section; the dotted areas of square section and circular section are shown in Figures 14(a) and 14(b), respectively; $A_{c,cut}$ is the largest cross-sectional area of concrete core at the opening section; the shadow areas of square section and circular section are shown in Figures 14(a) and 14(b), respectively.

The ultimate strength of the tested CFST specimens with hole in this paper was calculated by using equation (18) for the square specimens and equation (11) for the circular ones, and the comparisons between test results and EC4 predictions were listed in Table 1 and shown in Figure 15. For the CFST stub columns with hole, the mean values of N_{uc}/N_{ue} were 0.941 and 0.937, and the standard deviations were 0.089 and 0.143 for square and circular sections, respectively. The results clearly showed that the equations were reasonable for predicting the capacities of the specimens.

4. Conclusions

The behavior of axially loaded CFST stub columns with hole was experimentally investigated in this paper. Within the limitation of this study, the following conclusions can be drawn based on the experimental results:

(1) Compared to the normal reference specimens, the CFST stub columns with hole demonstrated a different typical failure mode, which were outward local buckling near the opening area due to the lower confining effect provided by the opening steel tube to the concrete core.

(2) The height of hole (h), the size of hole (d), the depth of hole (l), and the presence of concrete core have effects on the strength and ductility of the opening CFST columns. Generally, for both square and circular columns, the strength index SI and the ductility index DI decrease with the increase of h, d, and l. Compared with the reference opening hollow tubular columns, both the ultimate strength and the ductility of the CFST columns with hole were significantly increased due to the existence of the concrete core.

(3) The equations proposed by Eurocode 4 [21] are adopted and extended with respect to the effects of the size of hole (d) and the depth of hole (l) to predict the ultimate strength of the CFST columns with hole. The predicted results showed reasonable agreements with the test results.

Data Availability

All experiments in this paper were carried out in the Structural Engineering Laboratory of Shenyang Jianzhu University. The data in tables and in pictures used to support the findings of this study are included within the article.

Conflicts of Interest

All the authors declare that they have no conflicts of interest in this paper.

Acknowledgments

This research was part of Project 51708366 supported by the National Natural Science Foundation of China (NSFC) and the Program for the Natural Science Fund of Liaoning Province (no. 2020-MS-201). The financial supports are highly appreciated.

References

[1] J. Arbocz and C. D. Babcock, "The effect of general imperfections on the buckling of cylindrical shells," *Journal of Applied Mechanics*, vol. 36, no. 1, pp. 28–38, 1969.

[2] J. G. Teng and J. M. Rotter, "Buckling of pressurized axisymmetrically imperfect cylinders under axial loads," *Journal of Engineering Mechanics*, vol. 118, no. 2, pp. 229–247, 1992.

[3] I. Tutuncu, *Compressive Load and Buckling Response of Steel Pipelines during Earthquakes*, Ph.D. thesis, Cornell University, Ithaca, NY, 2001.

[4] I. Tutuncu and T. D. O'Rourke, "Compression behavior of nonslender cylindrical steel members with small and large-scale geometric imperfections," *Journal of Structural Engineering*, vol. 132, no. 8, pp. 1234–1241, 2006.

[5] J. F. Jullien and A. Limam, "Effects of openings of the buckling of cylindrical shells subjected to axial compression," *Thin-Walled Structures*, vol. 31, no. 1-3, pp. 187–202, 1998.

[6] A. Vaziri and H. E. Estekanchi, "Buckling of cracked cylindrical thin shells under combined internal pressure and axial compression," *Thin-Walled Structures*, vol. 44, no. 2, pp. 141–151, 2006.

[7] B. Prabu, A. V. Raviprakash, and A. Venkatraman, "Parametric study on buckling behaviour of dented short carbon steel cylindrical shell subjected to uniform axial compression," *Thin-Walled Structures*, vol. 48, no. 8, pp. 639–649, 2010.

[8] T. Ghanbari Ghazijahani, H. Jiao, and D. Holloway, "Plastic buckling of dented steel circular tubes under axial compression: an experimental study," *Thin-Walled Structures*, vol. 92, pp. 48–54, 2015.

[9] Z. Tao, B. Uy, F. Y. Liao, and L. H. Han, "Nonlinear analysis of concrete-filled square stainless steel stub columns under axial compression," *The Journal of Constructional Steel Research*, vol. 67, no. 11, pp. 1719–1732, 2006.

[10] Z.-w. Yu, F.-x. Ding, and C. S. Cai, "Experimental behavior of circular concrete-filled steel tube stub columns," *Journal of Constructional Steel Research*, vol. 63, no. 2, pp. 165–174, 2007.

[11] X. Chang, L. Fu, H.-B. Zhao, and Y.-B. Zhang, "Behaviors of axially loaded circular concrete-filled steel tube (CFT) stub columns with notch in steel tubes," *Thin-Walled Structures*, vol. 73, pp. 273–280, 2013.

[12] Z. Tao, M. Ghannam, T.-Y. Song, and L.-H. Han, "Experimental and numerical investigation of concrete-filled stainless steel columns exposed to fire," *Journal of Constructional Steel Research*, vol. 118, pp. 120–134, 2016.

[13] CECS 188-2019, *Technical Specification for Steel Tube-Reinforced Concrete Column Structure*, China Construction Standardization Association, Beijing, China, [in Chinese], 2019.

[14] W. H. Chen, J. S. Lei, M. Wang, and Z. Y. Liao, "Design and optimization of open hole of steel tube concrete composite column," *Journal of Southwest University of Science and Technology*, vol. 33, no. 3, pp. 48–54, 2018.

[15] L.-H. Han, Q.-X. Ren, and W. Li, "Tests on inclined, tapered and STS concrete-filled steel tubular (CFST) stub columns," *Journal of Constructional Steel Research*, vol. 66, no. 10, pp. 1186–1195, 2010.

[16] L.-H. Han, G.-H. Yao, and X.-L. Zhao, "Behavior and calculation on concrete-filled steel CHS (Circular Hollow Section) beam-columns," *Steel and Composite Structures*, vol. 4, no. 3, pp. 169–188, 2004.

[17] AIJ, *Recommendations for Design and Construction of Concrete Filled Steel Tubular Structures*, Architectural Institute of Japan (AIJ), Tokyo, Japan, 2008.

[18] ANSI/AISC360-10, *Specification for Structural Steel Buildings*, American Institute of Steel Construction (AISC), Chicago, Illinois, 2010.

[19] BS5400, *Steel, Concrete and Composite Bridges-Part5: Code of Practice for the Design of Composite Bridges*, British Standard Institution, British, Europe, 2005.

[20] DBJ/T13-51-2010, *Technical Specification for Concrete-Filled Steel Tubular Structures*, The Construction Department of Fujian Province, Fuzhou, China, [in Chinese], 2010.

[21] Eurocode 4, *Design of Composite Steel and Concrete Structures-Part 1.1: General Rules and Rules for Buildings. EN 1994-1-1: 2004*, European Committee for Standardization, Brussels, Belgium, 2004.

[22] Z. Tao, U. Y. Brian, L. H. Han, and S. H. He, "Design of concrete-filled steel tubular members according to the Australian Standard AS 5100 model and calibration," *Australian Journal of Structural Engineering*, vol. 8, no. 3, pp. 197–214, 2008.